Theory of a Quantum Scanning Microscope for Cold Atoms

D. Yang, C. Laflamme, D. V. Vasilyev, M. A. Baranov, and P. Zoller
Institute for Theoretical Physics, University of Innsbruck, A-6020 Innsbruck, Austria
and Institute for Quantum Optics and Quantum Information of the Austrian Academy of Sciences, A-6020 Innsbruck, Austria

(Received 6 September 2017; published 30 March 2018)

We propose and analyze a scanning microscope to monitor "live" the quantum dynamics of cold atoms in a cavity QED setup. The microscope measures the atomic density with subwavelength resolution via dispersive couplings to a cavity and homodyne detection within the framework of continuous measurement theory. We analyze two modes of operation. First, for a fixed focal point the microscope records the wave packet dynamics of atoms with time resolution set by the cavity lifetime. Second, a spatial scan of the microscope acts to map out the spatial density of stationary quantum states. Remarkably, in the latter case, for a good cavity limit, the microscope becomes an effective quantum nondemolition device, such that the spatial distribution of motional eigenstates can be measured backaction free in single scans, as an emergent quantum nondemolition measurement.

DOI: 10.1103/PhysRevLett.120.133601

Spatially resolved observation of individual atoms is a key ingredient in exploring quantum many-body dynamics with ultracold atoms. This is highlighted by the recent development of the quantum gas microscope [1] where fluorescence measurements provide us with single shot images of atoms in optical lattices. Fluorescence imaging is, however, an inherently destructive quantum measurement, as it is based on multiple resonant light scattering resulting in recoil heating (see, however, Ref. [2]). In contrast, quantum motion of cold atoms can also be observed in nondestructive, weak measurements, realizing the paradigm of continuous measurement of a quantum system [3–5]. Below we describe and analyze a quantum optical setup for a scanning atomic microscope employing dispersive interactions in a cavity QED (CQED) setup [6], where the goal is to achieve continuous observation of the density of cold atoms [7] with subwavelength resolution [8]. We will be interested in operating modes, where we either map out spatial densities of energy eigenstates in single scans as an emergent quantum nondemolition (QND) measurement [9,15] or we monitor at a fixed position the time-resolved response to "see" quantum motion of atoms.

The operating principle of the microscope is illustrated as a CQED setup in Fig. 1: We assume that an atom traversing the focal region of the microscope signals its presence with an internal spin flip; i.e., the position, and thus the motion of the atom, is correlated with its internal spin degree of freedom. While subwavelength spatial resolution can in principle be achieved by driving transition between spin states in the presence of external fields generating energy shifts with strong spatial gradients [16,17], this spatial resolution is typically accompanied with strong forces acting on the atom. Instead, we will describe below a setup with diminished disturbance, based on the position-dependent "dark state" in a Λ system [18], involving a pair of long-lived atomic ground state levels,

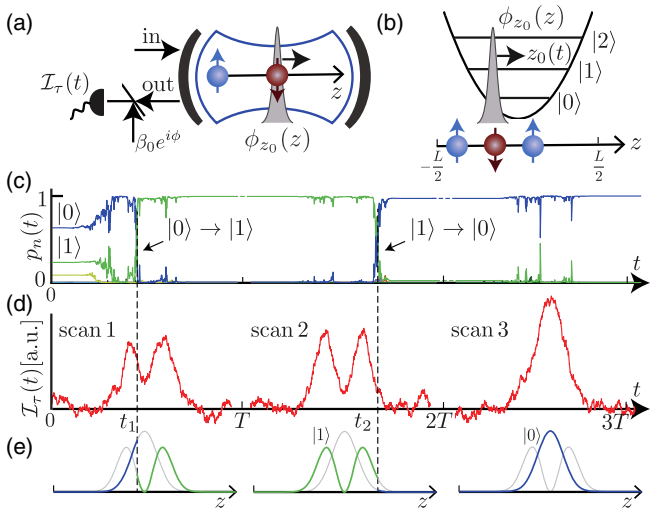

FIG. 1. (a) Scanning microscope as a CQED setup. The atom signals its presence in the focal region with subwavelength resolution as a spin flip, detected via a dispersive cavity coupling in homodyne measurement. (b) Spatial scan of the focal point $z_0 = z_0(t)$ for an atom in a harmonic oscillator (HO). (c)–(e) Operation of the microscope in the good cavity limit as emergent QND measurement (see text). For an atom in a thermal state of the HO we simulate a single measurement run involving three consecutive spatial scans: (c) conditional trap populations $p_n(t)$ $(n = 0, 1, 2)$ and (d) homodyne current $\mathcal{I}_\tau(t)$ in arbitrary unit (a.u.). QND measurement prepares the atom in a trap state $|n\rangle$, and $\mathcal{I}_\tau(t)$ traces the corresponding density (e) in the subsequent scan. Times t_1, t_2 indicate quantum jumps between trap states (see text).

 © 2018 American Physical Society

representing the spin. We can detect this spin flip nondestructively with a dispersive interaction, e.g., as a shift of a cavity mode of an optical resonator. Thus the atom traversing the focal region of the microscope, as defined by lasers generating the atomic dark state, becomes visible as a phase shift of the laser light reflected from the cavity. This phase shift is revealed in homodyne detection. Such CQED schemes are timely in view of both the recent progress with cold atoms in cavity and nanophotonic setups [19–27] and the growing interests in conditional dynamics of cold atoms under measurement [28–33].

Below we will develop a quantum optical model of continuous measurement [4,5,34] of atomic density, via measurement of the homodyne current for the setup described in Fig. 1. We adopt the language of the stochastic master equation (SME) for the conditional density matrix $\rho_c(t)$ of the joint atom-cavity system, which describes time evolution conditional to observation of a given homodyne current trajectory, as "seen" in a single run of an experiment, and including the backaction on the atom. This will allow us to address to what extent the observed homodyne current in a spatial scan provides a faithful measurement of atomic density and the expected signal-to-noise ratio (SNR).

Quantum optical model.—We consider a model system of an atom moving in 1D along the z axis, placed in a driven optical cavity. To detect the atom at z_0 with resolution σ, we introduce a spatially localized dispersive coupling of the atom to a single cavity mode of the form

$$\hat{H}_{\rm coup} = \phi_{z_0}(\hat{z})\hat{c}^\dagger\hat{c}. \tag{1}$$

Here, $\phi_{z_0}(z)$ defines a sharply peaked focusing function of support σ around z_0, and $\hat{c}^\dagger\hat{c}$ is the photon number operator for the cavity mode with destruction (creation) operators $\hat{c}(\hat{c}^\dagger)$. An implementation of $\phi_{z_0}(\hat{z})$ achieving optical subwavelength resolution $\sigma \ll \lambda$ based on atomic dark states in a Λ system will be described below. We find it convenient to write $\phi_{z_0}(z) \equiv \mathcal{A} f_{z_0}(z)$ with $f_{z_0}(z)$ normalized and $\mathcal{A}$ a constant with the dimensions of energy.

According to Eq. (1), the presence of an atom inside the focal region results in a shift of the cavity resonance. This can be detected with homodyne measurement, where the output field of the cavity is superimposed with a local oscillator with phase ϕ. The homodyne current can, for a single measurement trajectory, be written as $I(t) = \sqrt{\kappa}\langle\hat{X}_\phi\rangle_c + \xi(t)$, i.e., follows the expectation value of the quadrature operator of the intracavity field, $\hat{X}_\phi \equiv e^{i\phi}\hat{c}^\dagger + e^{-i\phi}\hat{c}$, up to the (white) shot noise $\xi(t)$. Here, κ represents the cavity damping rate and $\langle\cdots\rangle_c \equiv \mathrm{Tr}\{\ldots\rho_c(t)\}$ refers to an expectation value with respect to the conditional density matrix of the joint atom-cavity system.

On a more formal level, we write for the evolution under homodyne detection the Itô stochastic differential equations for the homodyne current,

$$dX_\phi(t) \equiv I(t)dt = \sqrt{\kappa}\langle\hat{X}_\phi\rangle_c dt + dW(t), \tag{2}$$

with $dW(t)$ Wiener noise increments, and the SME for the conditional density matrix,

$$d\rho_c = -\frac{i}{\hbar}[\hat{H},\rho_c]dt + \kappa\mathcal{D}[\hat{c}]\rho_c dt + \sqrt{\kappa}\mathcal{H}[\hat{c}e^{-i\phi}]\rho_c dW(t). \tag{3}$$

Equation (2) identifies the homodyne current as the measurement of the quadrature component $dX_\phi(t)$ of the output field in a time step $[t, t+dt)$. The SME Eq. (3) contains the total Hamiltonian $\hat{H} = \hat{H}_{\rm syst} + \hat{H}_c + \hat{H}_{\rm coup}$, with $\hat{H}_{\rm syst} = \hat{p}_z^2/2m + V(\hat{z})$ the Hamiltonian of the atomic system in an external potential V, $\hat{H}_c = i\hbar\sqrt{\kappa}\mathcal{E}(\hat{c} - \hat{c}^\dagger)$ the Hamiltonian for the driven cavity in the rotating frame (we assume resonant driving for simplicity), and $\mathcal{E}$ the coherent amplitude of the cavity mode driving field. The last two terms in Eq. (3) account for the backaction of homodyne measurement. The Lindblad operator $\mathcal{D}[\hat{c}]\rho \equiv \hat{c}\rho\hat{c}^\dagger - \frac{1}{2}\hat{c}^\dagger\hat{c}\rho - \frac{1}{2}\rho\hat{c}^\dagger\hat{c}$ describes the system decoherence (the cavity field damping) due to the coupling to the outside electromagnetic modes, and the nonlinear operator $\mathcal{H}[\hat{c}]\rho_c \equiv \hat{c}\rho_c - \langle\hat{c}\rangle_c\rho_c + \mathrm{H.c.}$ updates the density matrix conditioned on the observation of the homodyne photocurrent $I(t)$.

The relation between the homodyne current and the local atomic density is most transparent in the limit where the cavity response time $\tau_c = 1/\kappa$ is much faster than other timescales including atomic motion $\hat{H}_{\rm syst}$ and the dispersive coupling f_{z_0}, i.e., the bad cavity limit. Adiabatic elimination of the cavity gives

$$dX_\phi(t) \equiv I(t)dt = 2\sqrt{\gamma}\langle f_{z_0}(\hat{z})\rangle_c dt + dW(t), \tag{4}$$

with the atomic conditional density matrix $\tilde{\rho}_c(t)$ obeying the SME:

$$d\tilde{\rho}_c = -\frac{i}{\hbar}[\hat{H}_{\rm syst},\tilde{\rho}_c]dt + \gamma\mathcal{D}[f_{z_0}(\hat{z})]\tilde{\rho}_c dt + \sqrt{\gamma}\mathcal{H}[f_{z_0}(\hat{z})]\tilde{\rho}_c dW(t). \tag{5}$$

Here, $\gamma = [4\mathcal{A}\mathcal{E}/(\hbar\kappa)]^2$ is an effective measurement rate, and we have chosen $\phi = -\pi/2$ [11]. According to Eq. (4) the homodyne current $I(t)$ is a direct probe of the local atomic density at z_0 with spatial resolution σ [35]. Equations (4) and (5), or Eqs. (2) and (3) in the general case, provide us with the tools to study the dynamics of the "microscope" in various modes of operation (see below).

Instead of single trajectories, we can also consider ensemble averages corresponding to repeated preparation and measurement cycles. We define a density operator for the atom-cavity system $\rho(t) = \langle\rho_c(t)\rangle_{\rm st}$ as the statistical average over the conditional density matrices, and an

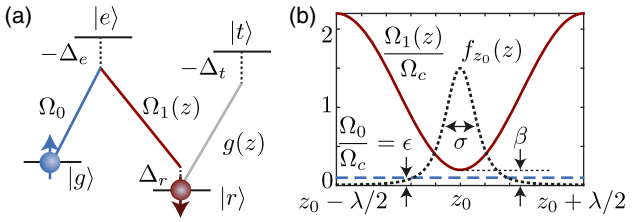

FIG. 2. Implementing the focusing function $\phi_{z_0}(z)$. (a) The Λ configuration $|g\rangle, |r\rangle, |e\rangle$ supporting a dark state with a subwavelength spin structure associated with the ground states (see text), and dispersive cavity coupling on the transition $|r\rangle \to |t\rangle$. (b) The Rabi frequencies, $\Omega_1(z) = \Omega_c\{1 + \beta - \cos[k(z - z_0)]\}$ (solid line), $\Omega_0 = \epsilon\Omega_c$ (dashed line), and the (dimensionless) focusing function $f_{z_0}(z)$ (dotted line) shown for $\epsilon = \beta/2 = 0.1$. For this configuration, the corresponding nonadiabatic potential [36,37] is strongly suppressed [11].

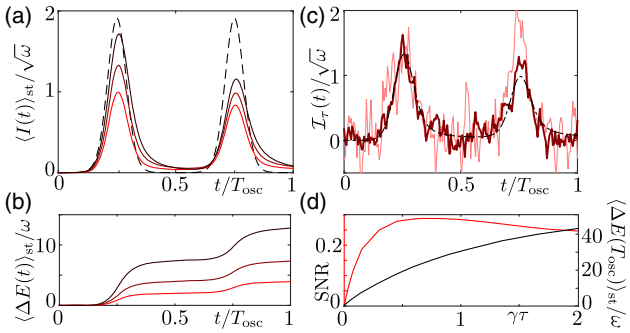

FIG. 3. Monitoring oscillations of a coherent wave packet in a HO ($\alpha = 2$) with a microscope at $z_0 = 0$ and $\sigma = 0.3\ell_0$. (a) The ensemble-averaged $\langle I(t)\rangle_{\rm st}$ over the oscillation period $T_{\rm osc} = 2\pi/\omega$ with increasing $\gamma/\omega = 1$, 2, and 4 (light to dark). Dashed line indicates the ideal (neglecting measurement backaction) transit signal for $\gamma/\omega = 4$. (b) Heating of the atom during measurements. (c) Filtered homodyne current for $\gamma = 2\omega$, averaged over 50 (thin) and 300 (thick) measurements. (d) SNR at the first peak ($t = T_{\rm osc}/4$) for a single measurement and the heating for different $\gamma\tau$, with τ the filter integration time (see text).

averaged homodyne current $\langle I(t)\rangle_{\rm st} = \sqrt{\kappa}{\rm Tr}\{\hat{X}_\phi\rho(t)\}$. This density operator obeys a master equation (ME), obtained from the SME Eq. (3) by averaging over trajectories. Thus, $\rho_c(t) \to \rho(t)$ in Eq. (3) with the stochastic term dropped according to the Itô property $\langle\ldots dW(t)\rangle_{\rm st} = 0$. An analogous ME for the atom $\tilde{\rho}(t) = \langle\tilde{\rho}_c(t)\rangle_{\rm st}$ can be derived from the adiabatically eliminated SME Eq. (5) [11].

Implementation of the focusing function $\phi_{z_0}(\hat{z})$.—The atom-cavity coupling Eq. (1) with subwavelength resolution can be achieved using the position-dependent dark state of a Λ system [18,36,37]. We consider the level scheme of Fig. 2(a), where two atomic ground (spin) states $|g\rangle$ and $|r\rangle$ are coupled to the excited state $|e\rangle$ with Rabi frequencies Ω_0 and $\Omega_1(z)$, respectively. This configuration supports a dark state $|D(z)\rangle = \sin\theta(z)|g\rangle - \cos\theta(z)|r\rangle$ with $\tan\theta(z) = \Omega_1(z)/\Omega_0$, which via destructive interference is decoupled from the dissipative excited state $|e\rangle$. We note that in spatial regions $\Omega_1(z) \gg \Omega_0$ the atom will be (dominantly) in state $|g\rangle$, while in regions $\Omega_1(z) \ll \Omega_0$ the atom will be in $|r\rangle$. This allows us to define via the spatial dependence of $\Omega_1(z)$ regions with subwavelength resolution $|z - z_0| \lesssim \sigma \ll \pi/k = \lambda/2$, characterized by atoms in $|r\rangle$. Atoms in $|r\rangle$ can be dispersively coupled to the cavity mode, resulting in a shift $g^2(z)/\Delta_t\hat{c}^\dagger\hat{c}$, with $g(z)$ the cavity coupling much smaller than the detuning Δ_t [cf. Fig. 2(a)]. Thus, atoms prepared in the dark state experience a shift [Eq. (1)] with

$$\phi_{z_0}(z) \equiv \mathcal{A}f_{z_0}(z) = \frac{\hbar g^2(z)}{\Delta_t}|\langle r|D(z)\rangle|^2 = \frac{\hbar g^2(z)}{\Delta_t}\cos^2\theta(z).$$

We illustrate this focusing function with subwavelength resolution in Fig. 2(b) for a specific laser configuration.

Microscope operation.—The parameters characterizing the microscope are the spatial resolution $\sigma \ll \lambda$, the temporal resolution τ_c (given essentially by the cavity linewidth $1/\kappa$), and the dispersive atom-cavity coupling controlling the strength of the measurement. To be specific, we illustrate below the operation of the microscope as continuous observation of an atom moving in a harmonic oscillator (HO) potential with an oscillation frequency ω and vibrational eigenstates $|n\rangle$ ($n = 0, 1, \ldots$). The generic physical realization includes a neutral atom in an optical trap (lattice), or an ion in a Paul trap [5], where we require a spatial resolution better than the length scale set by the HO ground state $\sigma \lesssim \ell_0 = \sqrt{\hbar/m\omega}$ with m the atomic mass.

We consider below two modes of operation. In the first, the microscope is placed at a given z_0, and we wish to "record a movie" of the time dynamics of an atomic wave packet (e.g., a coherent state) passing (repeatedly) through the observation zone. This requires a time resolution better than the oscillation period, and corresponds to the bad cavity limit $\kappa \gg \omega$, where according to Eq. (5) the homodyne current as a function of time mirrors directly the wave packet motion at z_0 (cf. Fig. 3 and discussion below). As the second case, we consider the good cavity limit $\kappa \ll \omega$. Here, the observed homodyne signal traces the atomic dynamics at z_0 cavity averaged over many oscillation periods [38]. However, as we show below, in this regime a slow scan of the focal point $z_0 \equiv z_0(t)$ across the spatial region of interest will turn the microscope into an effective QND device, which maps out the spatial density associated with a particular energy eigenfunction of the trapped particle with resolution σ. This will be discussed below in the context of Figs. 1(c)–1(e), where a particle is prepared initially in a state $\tilde{\rho}(0) = \sum_n p_n|n\rangle\langle n|$ (e.g., a thermal state), and in the spirit of QND measurements, a single scan with the microscope first collapses the atomic state into a particular motional eigenstate, and subsequently "takes a picture" of its spatial density. This ability of a

single scan to reveal the density of energy eigenfunctions is in contrast to the first case above, where the measurement is inherently destructive and a good SNR is only obtained with repeated runs of the experiment.

Bad cavity limit and time-resolved dynamics.—In Fig. 3(a) we plot the ensemble-averaged homodyne current $\langle I(t)\rangle_{\rm st}$ for a microscope positioned at $z_0 = 0$, which monitors the periodic motion of an atomic wave packet in the HO. The atom is initially prepared in a coherent state $|\alpha\rangle$ displaced from the trap center with $|\alpha| \gg 1$, and the microscope detects the transit of the wave packet with velocity $v = \sqrt{2}\ell_0|\alpha|\omega$ through the trap center at times $t = 1/4$, $3/4T_{\rm osc}$, etc., with $T_{\rm osc} = 2\pi/\omega$ the oscillator period. The time dependence of the homodyne current reveals the shape of the wave packet for the given resolution $\sigma = 0.3\ell_0$. Figure 3(a) plots $\langle I(t)\rangle_{\rm st} = 2\sqrt{\gamma}\,{\rm Tr}\{f_{z_0}(\hat{z})\tilde{\rho}(t)\}$ for increasing measurement strengths γ, with $\tilde{\rho}(t) \equiv \langle\tilde{\rho}_c(t)\rangle_{\rm st}$ obeying Eq. (5). For the given parameters, Fig. 3(a) displays the ability of the homodyne current to faithfully represent the temporal shape of the wave packet, and reveals the measurement backaction with increasing γ as a successive distortion of the signal with time. Figure 3(b) quantifies this backaction as an increase of the mean energy of the oscillator with time.

The SNR associated with these measurements is shown in Figs. 3(c) and 3(d). We define the SNR as $\langle\mathcal{I}_\tau(t)\rangle_{\rm st}^2/\langle\delta\mathcal{I}_\tau^2(t)\rangle_{\rm st}$ with $\mathcal{I}_\tau(t) \equiv \int_\tau I(t+t')dt'/\sqrt{\tau}$ the homodyne current Eq. (2) after a low-pass filter with bandwidth τ^{-1} and the variance $\langle\delta\mathcal{I}_\tau^2(t)\rangle_{\rm st} \equiv \langle\mathcal{I}_\tau^2(t)\rangle_{\rm st} - \langle\mathcal{I}_\tau(t)\rangle_{\rm st}^2$. We choose an integration time τ sufficiently long to suppress the shot noise, but short enough to resolve the temporal shape of the wave packet. An optimal τ is related to the microscope spatial resolution, $\tau \sim \sigma/v = (\sigma/\ell_0)\tau_{\rm tr}$, with $\tau_{\rm tr}$ the transit time of the wave packet through the focal region. In Fig. 3(c) we show the homodyne current $\mathcal{I}_\tau(t)$ averaged over an increasing number of measurements, and the convergence to the results of Fig. 3(a). In Fig. 3(d) the SNR in a single scan is plotted vs the measurement strength γ. It shows the general behavior of non-QND measurements [39]: For small γ, the SNR grows with increasing γ due to suppression of the shot noise. For large γ, SNR eventually drops down as the measurement backaction induces strong additional noises.

Good cavity limit as emergent QND measurement.—A QND measurement requires that the associated observable commutes with the system Hamiltonian. While $f_{z_0}(\hat{z})$ does not commute with $\hat{H}_{\rm syst}$, an effective QND measurement emerges in the good cavity limit $\kappa \ll \omega$. We can see this by transforming the SME Eq. (3) to an interaction picture with respect to $\hat{H}_{\rm syst}$. This transformation results in the replacement $f_{z_0}(\hat{z}) \to \sum_\ell \hat{f}_{z_0}^{(\ell)} e^{-i\ell\omega t}$, where $\hat{f}_{z_0}^{(\ell)} = \sum_n f_{n,n+\ell}|n\rangle\times\langle n+\ell|$, with $f_{mn} = \langle m|f_{z_0}(\hat{z})|n\rangle$. In a homodyne measurement, where the current $I(t)$ is monitored with time resolution $1/\kappa$, as filtered by the cavity, the terms rapidly oscillating with frequencies $\ell\omega$ (motional sidebands) will not be resolved. Thus, homodyne detection provides a continuous measurement of $\hat{f}_{z_0}^{(0)} = \sum_n f_{n,n}|n\rangle\langle n|$ representing the emergent QND observable [10].

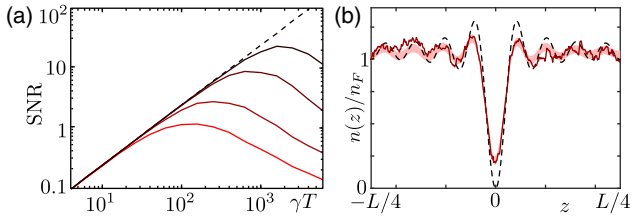

FIG. 4. Single-run scans in the QND regime. (a) SNR vs γT for a scan of an atom initialized in the state $|1\rangle$ of a HO for $\kappa/\omega = 10$, 1, 0.25, 0.1 (light to dark), compared to an ideal QND measurement (dashed line) for $\sigma = 0.3\ell_0$ and $L = 8\ell_0$. SNR is taken at $z_0(t) = -\ell_0$ (theoretical maximum). (b) Scan of Friedel oscillations for $N = 16$ noninteracting fermions in a box of length L due to an impurity at $z = 0$: the scanning signal (solid line), the total noise variance (shaded area), and the theoretical density profile $n(z) = n_F[1 - \sin(2k_F z)/(2k_F z)]$ (dashed line), with $n_F = k_F/\pi = N/L$.

A formal derivation of these results is provided in Ref. [11] starting from the SME Eq. (3). There we derive for the homodyne current $dX_\phi(t) \equiv I(t)dt = 2\sqrt{\gamma}\langle\hat{f}_{z_0}^{(0)}\rangle_c + dW(t)$ with $\langle\cdots\rangle_c = {\rm Tr}\{\ldots\tilde{\rho}_c(t)\}$, where the conditional density operator $\tilde{\rho}_c(t)$ obeys the SME,

$$d\tilde{\rho}_c = -\frac{i}{\hbar}[\hat{H}_{\rm syst},\tilde{\rho}_c]dt + \sum_{\ell\neq 0}\frac{\gamma}{1+(2\omega\ell/\kappa)^2}\mathcal{D}[\hat{f}_{z_0}^{(\ell)}]\tilde{\rho}_c dt + \gamma\mathcal{D}[\hat{f}_{z_0}^{(0)}]\tilde{\rho}_c dt + \sqrt{\gamma}\mathcal{H}[\hat{f}_{z_0}^{(0)}]\tilde{\rho}_c dW(t), \tag{6}$$

with γ the measurement strength defined above (assuming resonant driving). To provide a physical interpretation, we take matrix elements of Eq. (6) in the energy eigenbases and obtain a (nonlinear) stochastic rate equation for the trap-state populations $p_n = \langle n|\tilde{\rho}_c|n\rangle$:

$$dp_n = \frac{\gamma}{1+(2\omega/\kappa)^2}[A_n^{(+)}p_{n+1} + A_n^{(-)}p_{n-1} - B_n p_n]dt + 2\sqrt{\gamma}p_n\left(f_{nn} - \sum_m f_{mm}p_m\right)dW(t). \tag{7}$$

Here, $A_n^{(\pm)} \equiv |f_{n,n\pm1}|^2$, $B_n \equiv A_n^{(+)} + A_n^{(-)}$, and for simplicity we have kept only the dominant terms $\ell = 0, \pm 1$ for $\kappa/\omega \ll 1$. We emphasize that Eq. (7) involves two timescales. The stochastic term in the second line describes the collapse of the density operator to a particular trap eigenstate $\tilde{\rho}_c(t) \to |n\rangle\langle n|$ within a collapse time $T_{\rm coll} \sim 1/\gamma$. In contrast, the first line is a redistribution of population between the trap levels, for a much longer dwell time, $T_{\rm dwell} \sim (2\omega/\kappa)^2\gamma^{-1} \gg T_{\rm coll}$. As a result, the time evolution consists of a rapid collapse to an energy

eigenstate $|n\rangle$, followed by a sequence of rare quantum jumps $n \to n \pm 1$ on the timescale T_{dwell}. The QND mode of the microscope exploits these two timescales by scanning the focal point across the system, $-L/2 < z_0(t) < L/2$, in a time $T_{\mathrm{coll}} \ll T \lesssim T_{\mathrm{dwell}}$. Starting the measurement scan, the motional state will first collapse to a particular state $|n\rangle$, with the subsequent scan revealing the spatial density profile $\langle n|\hat{f}^{(0)}_{z_0}|n\rangle = \int dz f_{z_0}(z)|\langle z|n\rangle|^2$.

Figure 1(c) shows a simulation representing a single run in the QND regime ($\kappa/\omega = 0.1$) based on integrating the SME Eq. (6). The atom at $t = 0$ is prepared in a thermal motional state of the HO, $\tilde{\rho}(0) = \sum_n p_n|n\rangle\langle n|$, with $n_{\mathrm{th}} = 0.6$. We perform three consecutive spatial scans covering $-L/2 < z_0(t) < L/2$ ($L = 10\ell_0$), each in a time interval T ($\gamma T = 5000$). For the run shown in Figs. 1(c)–1(e), the QND measurement in scan 1 first projects the atomic trap population into $|0\rangle$, followed by a transition to $|1\rangle$ at time t_1, and $|1\rangle \to |0\rangle$ at t_2 in scan 2, and no transition in scan 3. The homodyne current $\mathcal{I}_\tau(t)$ associated with these single scans is a faithful representation of the spatial density distributions of eigenfunctions $|\langle z|n\rangle|^2$. In Fig. 4(a) the SNR of single scans of a pure state is shown against the (dimensionless) measurement strength γT. By decreasing κ/ω we greatly suppress the measurement backaction, rendering them into rarer quantum jumps, thus improving the SNR.

The concept of a scanning microscope to observe *in vivo* cold atom dynamics is readily adapted to a quantum many-body system, and we show in Fig. 4(b) a single spatial scan of the Friedel oscillation of a noninteracting Fermi sea in the presence of a single impurity [11]. While we have focused on homodyne measurement in CQED for continuous readout (with experimental feasibility discussed in Ref. [11]), atomic physics setups provide interesting alternative routes to achieve weak continuous measurement, e.g., coupling to atomic ensembles via Rydberg interactions [40–42].

We acknowledge discussions with P. Hauke, and thank P. Grangier, I. B. Mekhov, K. Mølmer, and L. Orozco for useful comments on the manuscript. Work at Innsbruck is supported by the Austrian Science Fund SFB FoQuS (FWF Project No. F4016-N23) and the European Research Council (ERC) Synergy Grant UQUAM.

[1] For a review, see S. Kuhr, Natl. Sci. Rev. **3**, 170 (2016), and references therein.
[2] Y. Ashida and M. Ueda, Phys. Rev. Lett. **115**, 095301 (2015).
[3] V. B. Braginsky and F. Y. Khalili, *Quantum Measurement* (Cambridge University Press, Cambridge, England, 1992).
[4] H. M. Wiseman and G. J. Milburn, *Quantum Measurement and Control* (Cambridge University Press, Cambridge, England, 2009).
[5] C. Gardiner and P. Zoller, *The Quantum World of Ultra-Cold Atoms and Light Book II* (Imperial College Press, London, 2015).
[6] For recent reviews, see I. B. Mekhov and H. Ritsch, J. Phys. B **45**, 102001 (2012); H. Ritsch, P. Domokos, F. Brennecke, and T. Esslinger, Rev. Mod. Phys. **85**, 553 (2013); T. E. Northup and R. Blatt, Nat. Photonics **8**, 356 (2014); A. Reiserer and G. Rempe, Rev. Mod. Phys. **87**, 1379 (2015).
[7] Continuous observation of classical atomic motion in cavity QED is demonstrated in C. J. Hood, T. W. Lynn, A. C. Doherty, A. S. Parkins, and H. J. Kimble, Science **287**, 1447 (2000); T. Puppe, I. Schuster, A. Grothe, A. Kubanek, K. Murr, P. W. H. Pinkse, and G. Rempe, Phys. Rev. Lett. **99**, 013002 (2007); M. L. Terraciano, R. Olson Knell, D. G. Norris, J. Jing, A. Fernandez, and L. A. Orozco, Nat. Phys. **5**, 480 (2009).
[8] Strong measurement of quantum particles with subwavelength resolution is demonstrated, e.g., in P. C. Maurer, J. R. Maze, P. L. Stanwix, L. Jiang, A. V. Gorshkov, A. A. Zibrov, B. Harke, J. S. Hodges, A. S. Zibrov, A. Yacoby, D. Twitchen, S. W. Hell, R. L. Walsworth, and M. D. Lukin, Nat. Phys. **6**, 912 (2010); F. Zähringer, G. Kirchmair, R. Gerritsma, E. Solano, R. Blatt, and C. F. Roos, Phys. Rev. Lett. **104**, 100503 (2010).
[9] Note that the local density operator does not commute with the Hamiltonian. Nevertheless, in our setup, we can measure local densities for energy eigenstates with no backaction—an emergent QND measurement; see text and Ref. [10].
[10] The concept of emergent QND observable and measurement can be defined in a general context, as detailed in Ref. [11].
[11] See Supplemental Material at http://link.aps.org/supplemental/10.1103/PhysRevLett.120.133601 for an extended discussion on emergent QND measurement, implementation of the focusing function, derivation of the stochastic master equations, scanning the Friedel oscillation and experimental feasibility. The Supplemental Material includes Refs. [12–14].
[12] D. Yang *et al.* (to be published).
[13] C. J. Hood, M. S. Chapman, T. W. Lynn, and H. J. Kimble, Phys. Rev. Lett. **80**, 4157 (1998).
[14] O. Černotík, D. V. Vasilyev, and K. Hammerer, Phys. Rev. A **92**, 012124 (2015).
[15] For QND measurements in quantum optics, see, e.g., S. Gleyzes, S. Kuhr, C. Guerlin, J. Bernu, S. Deleglise, U. B. Hoff, M. Brune, J.-M. Raimond, and S. Haroche, Nature (London) **446**, 297 (2007); B. R. Johnson, M. D. Reed, A. A. Houck, D. I. Schuster, L. S. Bishop, E. Ginossar, J. M. Gambetta, L. DiCarlo, L. Frunzio, S. M. Girvin, and R. J. Schoelkopf, Nat. Phys. **6**, 663 (2010); J. Volz, R. Gehr, G. Dubois, J. Estève, and J. Reichel, Nature (London) **475**, 210 (2011); G. Barontini, L. Hohmann, F. Haas, J. Estève, and J. Reichel, Science **349**, 1317 (2015); C. B. Møller, R. A. Thomas, G. Vasilakis, E. Zeuthen, Y. Tsaturyan, M. Balabas, K. Jensen, A. Schliesser, K. Hammerer, and E. S. Polzik, Nature (London) **547**, 191 (2017).
[16] K. D. Stokes, C. Schnurr, J. R. Gardner, M. Marable, G. R. Welch, and J. E. Thomas, Phys. Rev. Lett. **67**, 1997 (1991).
[17] C. Weitenberg, M. Endres, J. F. Sherson, M. Cheneau, P. Schausz, T. Fukuhara, I. Bloch, and S. Kuhr, Nature (London) **471**, 319 (2011).

[18] A. V. Gorshkov, L. Jiang, M. Greiner, P. Zoller, and M. D. Lukin, Phys. Rev. Lett. **100**, 093005 (2008).
[19] A. Stute, B. Casabone, P. Schindler, T. Monz, P. O. Schmidt, B. Brandstatter, T. E. Northup, and R. Blatt, Nature (London) **485**, 482 (2012).
[20] M. Wolke, J. Klinner, H. Keßler, and A. Hemmerich, Science **337**, 75 (2012).
[21] B. Hacker, S. Welte, G. Rempe, and S. Ritter, Nature (London) **536**, 193 (2016).
[22] J. Léonard, A. Morales, P. Zupancic, T. Esslinger, and T. Donner, Nature (London) **543**, 87 (2017).
[23] A. J. Kollár, A. T. Papageorge, V. D. Vaidya, Y. Guo, J. Keeling, and B. L. Lev, Nat. Commun. **8**, 14386 (2017).
[24] J. D. Thompson, T. G. Tiecke, N. P. de Leon, J. Feist, A. V. Akimov, M. Gullans, A. S. Zibrov, V. Vuletić, and M. D. Lukin, Science **340**, 1202 (2013).
[25] C. Junge, D. O'Shea, J. Volz, and A. Rauschenbeutel, Phys. Rev. Lett. **110**, 213604 (2013).
[26] A. Goban, C.-L. Hung, S.-P. Yu, J. D. Hood, J. A. Muniz, J. H. Lee, M. J. Martin, A. C. McClung, K. S. Choi, D. E. Chang, O. Painter, and H. J. Kimble, Nat. Commun. **5**, 3808 (2014).
[27] H. L. Sørensen, J.-B. Béguin, K. W. Kluge, I. Iakoupov, A. S. Sørensen, J. H. Müller, E. S. Polzik, and J. Appel, Phys. Rev. Lett. **117**, 133604 (2016).
[28] D. A. Steck, K. Jacobs, H. Mabuchi, T. Bhattacharya, and S. Habib, Phys. Rev. Lett. **92**, 223004 (2004).
[29] M. D. Lee and J. Ruostekoski, Phys. Rev. A **90**, 023628 (2014).
[30] A. C. J. Wade, J. F. Sherson, and K. Mølmer, Phys. Rev. Lett. **115**, 060401 (2015).
[31] G. Mazzucchi, S. F. Caballero-Benitez, D. A. Ivanov, and I. B. Mekhov, Optica **3**, 1213 (2016).
[32] Y. Ashida and M. Ueda, Phys. Rev. A **95**, 022124 (2017).
[33] C. Laflamme, D. Yang, and P. Zoller, Phys. Rev. A **95**, 043843 (2017).
[34] H. Carmichael, *An Open Systems Approach to Quantum Optics* (Springer, Berlin, 1993).
[35] We contrast this to schemes where $I(t)$ reflects the atomic positon $\langle\hat{z}\rangle_c$ in, e.g., R. Quadt, M. Collett, and D. F. Walls, Phys. Rev. Lett. **74**, 351 (1995); T. Konrad, A. Rothe, F. Petruccione, and L. Diósi, New J. Phys. **12**, 043038 (2010).
[36] M. Łacki, M. A. Baranov, H. Pichler, and P. Zoller, Phys. Rev. Lett. **117**, 233001 (2016).
[37] F. Jendrzejewski, S. Eckel, T. G. Tiecke, G. Juzelinas, G. K. Campbell, L. Jiang, and A. V. Gorshkov, Phys. Rev. A **94**, 063422 (2016).
[38] This situation is reminiscent of the sideband resolved laser cooling of trapped particles in the Lamb-Dicke limit where $\gamma \ll \omega$ with γ optical pumping rate [5].
[39] A. A. Clerk, M. H. Devoret, S. M. Girvin, F. Marquardt, and R. J. Schoelkopf, Rev. Mod. Phys. **82**, 1155 (2010).
[40] M. Saffman, T. G. Walker, and K. Mølmer, Rev. Mod. Phys. **82**, 2313 (2010).
[41] H. Labuhn, D. Barredo, S. Ravets, S. de Léséleuc, T. Macrì, T. Lahaye, and A. Browaeys, Nature (London) **534**, 667 (2016).
[42] H. Bernien, S. Schwartz, A. Keesling, H. Levine, A. Omran, H. Pichler, S. Choi, A. S. Zibrov, M. Endres, M. Greiner, V. Vuletić, and M. D. Lukin, Nature (London) **551**, 579 (2017).